Pioneer. Adv. Mater. 2025, 1(3): 1-15 DOI: 10.48308/piadm.2026.243252.1014

Shahid Beheshti University

Pioneering Advances in Materials

Journal homepage: http://piadm.sbu.ac.ir ISSN: 3115-7114

Research paper

XRD Phase Analysis and Residual Stress Evaluation of Cr–Zr-Based Coatings for Accident Tolerant Fuel Cladding

N. Yasavol[1], A. Raeisdana[1], M. Mohsenabadi[2]

[1]Plasma and Nuclear Fusion Research School, Nuclear Science and Technology Research Institute (NSTRI) Atomic Energy Organization of Iran, Tehran, Iran
[2]Nuclear Science and Technology Research Institute (NSTRI)

nyasavol@aeoi.org.ir

Article info:

Article history:

Received: 18/01/2026

Accepted: 19/02/2026

Keywords: Accident tolerant fuel (ATF); X-ray diffraction (XRD); Residual stress; Oxide phase transformation; Cr_2O_3; Zirconia (t-ZrO_2 and m-ZrO_2); Hardness estimation

Abstract

This study investigates the chromium (Cr) coating deposited onto Zr cladding using the IR-MPF-100 plasma focus device. The primary objective was the quantitative assessment of phases and residual stresses at the nanoscale, linking them directly to strengthening mechanisms. X-ray diffraction (XRD) analysis confirmed the formation of $Cr_2O_3$and ZrO_2 phases, with tetragonal and monoclinic ZrO_2 coexisting within the oxide scale. Crucially, residual compressive stresses, determined from XRD peak shifts, revealed that the Cr_2O_3 phase exhibits the highest compressive stress and effective hardness. Conversely, monoclinic ZrO_2 displayed the lowest values due to transformation-induced stress relaxation during cooling. Modeling demonstrated that the coating's elevated Taylor and Hall–Petch stresses, resulting from high dislocation density and nanoscale grain size, manifest as these large compressive residual stresses. The Zr substrate played a minor role, acting primarily as a stress-accommodating medium. These findings provide a critical quantitative understanding of stress-strengthening interdependence in advanced Cr–Zr coating systems.

1. Introduction

The mechanical integrity of accident tolerant fuel (ATF) cladding under both normal operating conditions and accident scenarios is a key requirement for advanced nuclear fuel systems. Chromium-based coatings deposited on zirconium alloy claddings have been widely investigated as promising ATF concepts due to their superior oxidation resistance, high melting temperature, and favorable compatibility with zirconium substrates [1, 2]. Beyond corrosion protection, however, the mechanical properties of these coatings and their oxide layers critically influence

coating adhesion, crack resistance, and long-term durability.

During high-temperature oxidation, Cr-coated zirconium claddings form multilayered oxide scales composed primarily of chromium oxide (Cr_2O_3) and zirconium dioxide (ZrO_2). Zirconia may exist in tetragonal (t-ZrO_2) and monoclinic (m-ZrO_2) phases, each exhibiting distinct elastic moduli, transformation strains, and mechanical response [3, 4]. The tetragonal-to-monoclinic (t → m) phase transformation, accompanied by a volume expansion of approximately 3–5%, plays a crucial role in stress relaxation and crack shielding, but may also contribute to microcracking under constrained conditions [4, 5]. Residual stresses develop in Cr-based coatings and their oxide layers due to coating deposition, thermal mismatch, oxidation-induced volume changes, and phase transformations. Compressive residual stresses within the Cr_2O_3 layer are generally beneficial for suppressing crack initiation and improving scale adherence, whereas tensile stresses within ZrO_2 layers may accelerate damage accumulation and spallation [6, 7]. Accurate quantification of phase-specific residual stresses is therefore essential for predicting coating reliability under thermo-mechanical loading relevant to loss-of-coolant accident (LOCA) and post-LOCA conditions.

Mechanical properties such as elastic–plastic behavior and hardness further reflect the hierarchical nature of the oxide system. Cr_2O_3 typically exhibits high stiffness and hardness due to strong ionic–covalent bonding, while ZrO_2 phases demonstrate lower hardness and greater strain accommodation capability [8, 9]. Experimental and modeling studies have shown that a gradual reduction in hardness from the coating surface toward the zirconium substrate can enhance damage tolerance by reducing stress concentrations at interfaces [10, 11].

X-ray diffraction (XRD) provides a powerful, non-destructive methodology for phase identification, lattice strain measurement, and residual stress evaluation in multiphase coating systems (Noyan & Cohen, 2013). When combined with elastic constants and micromechanical models, XRD-derived strain data can be correlated with yield stress, stress–strain behavior, and hardness, enabling a quantitative structure–property relationship to be established for Cr–Zr based ATF coatings. Such an approach offers valuable insight into the mechanical stability and performance limits of coated claddings under demanding nuclear service environments.

Prior research focusing on oxide layers formed via plasma processes, especially on Zr cladding, often characterized phases or residual stresses in isolation. A significant gap existed in quantitatively linking the high compressive residual stresses, induced specifically by the Plasma Focus technique, to the resultant phase-dependent effective hardness (and overall coating strength). Furthermore, the precise role of the ZrO_2 monoclinic phase in stress relaxation under these conditions was not fully elucidated.

Our study directly bridges this gap by (1) using the Plasma Focus method to achieve a specific, high level of compressive stress in the Cr_2O_3 layer, (2) employing XRD analysis to simultaneously measure the magnitude of these stresses and the phase-specific hardness, and (3) providing the first quantitative evidence that the high density of lattice defects (dislocations and nanoparticles) responsible for the Taylor/Hall-Petch strengthening mechanism directly translates into the measured high compressive stress state observed via XRD. This integrated approach provides a pathway for tailoring Cr coatings for enhanced wear resistance in nuclear applications."

2. Experimental Methods

2.1. Coating Deposition

Chromium–zirconium-based coatings were deposited on zirconium substrates using a pulsed

plasma deposition system. Figure 1 schematically illustrates the experimental setup employed in this study. The system consists of a high-voltage capacitor bank connected to the discharge chamber through a spark gap, enabling rapid energy release and plasma generation. The discharge current was monitored using a Rogowski coil, while voltage and current waveforms were recorded by a digital oscilloscope synchronized with the discharge pulse.

The discharge chamber was evacuated to a base pressure of approximately 10^{-3} mbar prior to plasma generation. High-voltage pulses were applied between the central anode and the surrounding cathode, leading to plasma formation and subsequent pinch compression in the inter-electrode region. The plasma pinch provided a highly energetic environment suitable for coating formation on the substrate surface.

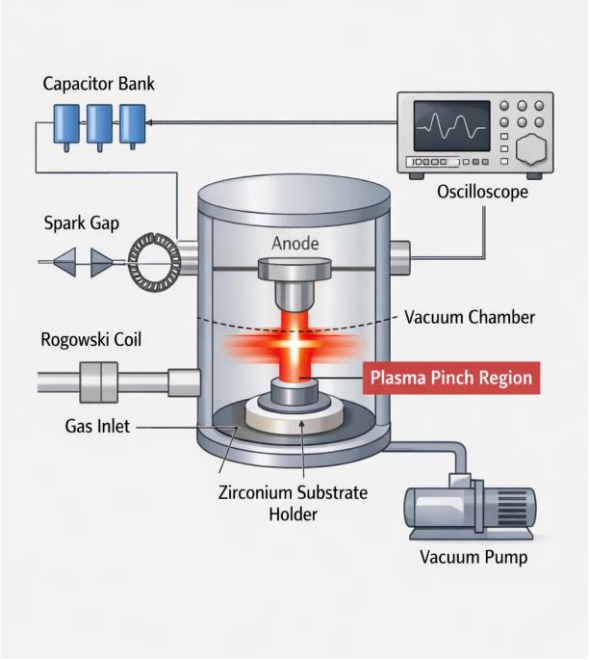

Figure 1. Schematic of the IR-MPF-100 plasma focus device. Installation of chromium in the anode head area and placement of the zirconium substrate at a distance of 35 cm away from the anode head

According to Figure 2, Zirconium samples were mounted on a sample holder positioned directly below the plasma pinch region to ensure effective exposure to the plasma flux. Repeated pulsed discharges resulted in the deposition of Cr–Zr coatings on the zirconium substrates. The deposition parameters, including discharge voltage, capacitor bank energy, and number of pulses, were kept constant throughout the experiments to ensure reproducibility. Phase composition of the as-deposited and oxidized coatings was analyzed using X-ray diffraction (XRD).

For the X-ray diffraction (XRD) experiment setup, the scanning will commence at an initial 2θ position of 30.0000°, extending to a final position of 90.0000°. The analysis will employ a step size of 0.0400° 2θ, with each measurement step being allotted a duration of 1.0000 seconds, utilizing the wavelength of copper Kα radiation, which is 1.5406 Å.

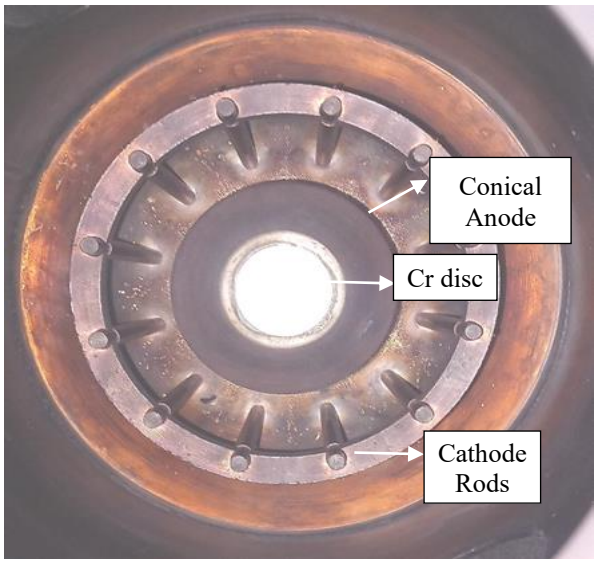

Figure 2. Bottom-up view of the anode and cathode. Pure chromium is installed in the anode head area

3. Results and discussions

3.1. Phase Identification and X-ray Diffraction Analysis

Figure 3 presents the X-ray diffraction patterns of the Cr–Zr–based coating with thickness of 50 μm

deposited on zirconium cladding. In this figure the related Zr peaks of the substrate decreased severely which is representative of Cr implantation and diffusion of Cr into the substrate. Moreover, chromium oxide (Cr_2O_3) and zirconium dioxide (ZrO_2) phases are recognized in Cr coating. Both tetragonal (t-ZrO_2) and monoclinic (m-ZrO_2) zirconia phases were identified based on their characteristic diffraction peaks. The diffraction peaks confirm the formation of crystalline Cr_2O_3 and ZrO_2 phases, in agreement with previous reports on chromium-coated accident tolerant fuel cladding systems [12, 13]. The ZrO_2 layer is dominated by the tetragonal phase, which is commonly stabilized in Cr-based coatings due to residual compressive stresses and nanocrystalline grain size (Cao & Ouyang, 2017; Zhao et al., 2021).

Although distinct monoclinic ZrO_2 reflections are weak, their formation is expected during thermal exposure and stress relaxation regimes typical of nuclear operating conditions [14].

Peak broadening analysis derived from XRD was performed to estimate crystallite size and microstrain.

The full width at half maximum (FWHM) values were corrected for instrumental broadening prior to analysis. All data derived from XRD calculated based on the known mechanical models, are listed in Table 1.

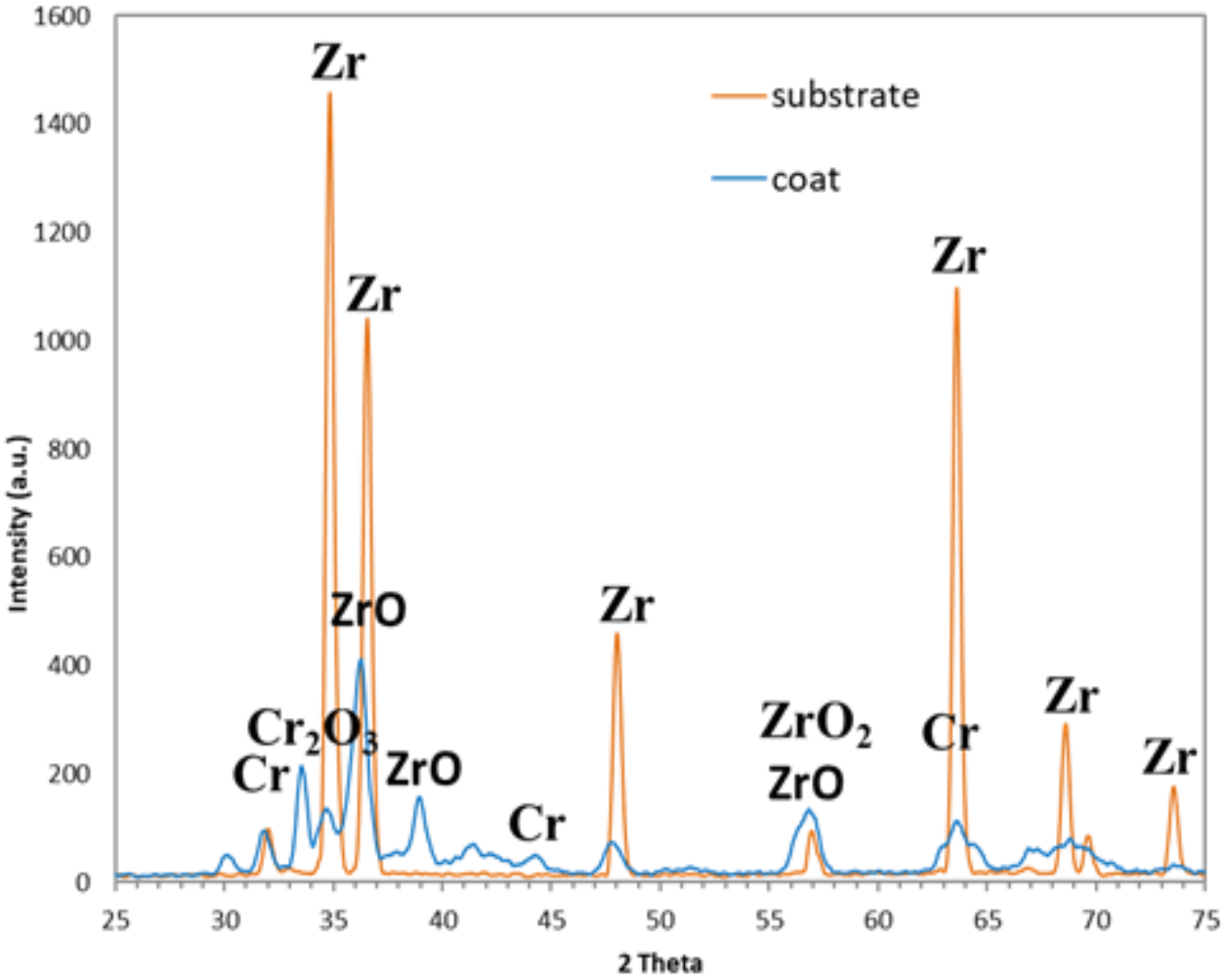

Figure 3. XRD of the substrate and the Cr coating peaks including chromium oxide (Cr_2O_3) and zirconium dioxide (ZrO_2)

3.2. Lattice strain determination

Lattice strain values were determined from the peak shift analysis of multiple diffraction planes using XRD. The lattice strain (ε) for selected crystallographic planes was calculated from the shift in diffraction peak positions according to the known equation as follows:

$$\varepsilon = \frac{d - d_0}{d_0}$$

where d and d_0 represent the measured and stress-free interplanar spacings, respectively.

Tetragonal ZrO_2 phase exhibited lattice strain values ranging from 0.23×10^{-3} to 0.58×10^{-3}, resulting in an average lattice strain of $\bar{\varepsilon}_{t-ZrO2}\approx0.41\times10^{-3}$. Such strain levels are consistent with residual stresses typically observed in oxide layers formed on chromium-coated zirconium claddings [15, 16]. The lattice strain of monoclinic ZrO_2 was derived from the XRD-measured strain values of tetragonal ZrO_2 peaks due to the absence of distinct monoclinic reflections and their comparable crystallographic response. The calculated average lattice strain of approximately 0.41×10^{-3} resulted in a residual stress of about 70 MPa for the monoclinic phase [17, 18].

3.3. Residual stress measurement

In this report, three related but distinct sources concerning to residual stress measurements were calculated in Cr–Zr coatings and their oxide systems including: 1) Taylor elastic stress (dislocation-based), 2) Hall–Petch strengthening [19] (grain boundary-based) and 3) Holm / Williamson–Hall microstrain (lattice distortion-based) and compared to each other. These three sources are not independent but are indirectly connected through XRD.

1. Stress caused by dislocation density assed by Taylor relation:

$$\sigma_{HP} = \sigma_0 + k_y D^{-1/2}$$

where is Taylor factor (≈ 2.7–3.1) (M≈3.06 (M metallic BCC of Cr)), α is constant of ≈0.2–0.4, G is the shear module, b is Bergere's vector and ρ is dislocation density (from XRD peak broadening). It is necessary to note that, although Taylor stress is often referred to as elastic, its origin is inherently dislocation-based. The elastic interaction fields of immobile dislocations give rise to a measurable lattice microstrain, which demonstrates residual stress in XRD measurements without requiring plastic deformation Derived data from XRD in Table 1. depict that for Coatings of (Cr_2O_3 + t-ZrO_2), very high dislocation density of (10^{14}–10^{15} m^{-2}), high G (Cr_2O_3 ≈ 140 GPa, t-ZrO_2 ≈ 70–80 GPa) and high Taylor stress (hundreds of MPa) were obtained. Taylor stress is a major contributor to compressive residual stress and hardness in the coating. In contrast, in Zr substrate, ρ (10^{12}–10^{13} m^{-2}), shear modulus, and Taylor stress are significantly smaller than those of the coating. As a result, the substrate mainly accommodates elastic mismatch; it does not control hardness [20, 21] .

2. Hall–Petch Strengthening (Grain Size Controlled):

$$\sigma_{HP} = \sigma_0 + k_y D^{-1/2}$$

where D is crystallite size (from Scherrer / W–H analysis), σ_y is yield stress, σ_0 is the lattice friction stress and ky is constant of Hall–Petch formula. For Cr-based coatings σ_0≈200–300 MPa and k_y is ≈0.4–0.6 $Mpa^{1/2}$ This relationship is the main bridge between the XRD data and mechanical properties. As shown in Table 1, in coating, nanocrystalline grains (20–60 nm), very high $d^{-1/2}$, as a result, strong Hall–Petch strengthening was gained. It means that grain boundaries act as dislocation barriers, stress accumulation sites and increase compressive stress. While in substrae (Zr) with micronsized grains, Hall–Petch term is weak, consequently, plastic deformation dominates instead of strengthening. Therefore, Hall–Petch effect is dominant in the coating, negligible in the substrate [22, 23]. The reduced

residual stress in the monoclinic ZrO_2 phase suggests enhanced mechanical stability of the oxide scale. Stress relaxation induced by the t→m phase transformation is expected to suppress crack initiation and interfacial delamination, thereby improving the integrity of Cr–Zr–based coatings under thermal transients and irradiation environments [14, 24].

3. Holm / Williamson–Hall microstrain (elastic lattice distortion)

Williamson–Hall relation:

$$\beta\cos\theta=\frac{k\lambda}{D}+4\varepsilon\sin\theta$$

Microstrain:

$$\varepsilon\sim\sqrt{\rho}$$

According to this model and Table 2, it can be implied that the substrate, with much lower microstrain acts as stress sink and there were no significant XRD peak asymmetry [25, 26]. In coating, high microstrain (10^{-4}–10^{-3}) originated by lattice mismatch (Cr_2O_3 / ZrO_2 / Cr), oxygen incorporation, phase coexistence (t-ZrO_2 ↔ m-ZrO_2) induced high residual stress. Theoretically it is known that the calculated stresses originate from lattice strain induced by deposition processes, thermal mismatch, and phase transformations occurring during oxidation. In this regard, the residual stress values in individual phases are described as be bellow: Metallic Cr coatings typically exhibit compressive residual stresses in the range of approximately −150 to −250 MPa. These stresses are mainly attributed to energetic particle bombardment during plasma focused Cr ions implantations, atomic peening effects, and lattice mismatch with the substrate [27]. The Cr_2O_3 phase shows a moderate compressive residual stress of about −98 MPa, as calculated from XRD lattice strain ($\varepsilon \approx 4.3 \times 10^{-4}$). Compared to metallic Cr, Cr_2O_3 exhibits reduced residual stress due to its more isotropic corundum crystal structure and the ability of grain boundaries to accommodate strain [28]. Metallic zirconium typically presents lower compressive stresses, in the range of −50 to −120 MPa. This behavior is related to its hexagonal close-packed (hcp) structure and relatively lower elastic modulus, which facilitates stress relaxation during film growth [29]. The highest compressive residual stresses are observed in tetragonal zirconia, reaching approximately −200 to −400 MPa. This elevated stress level arises from lattice distortion, thermal expansion mismatch, and stress-induced stabilization of the tetragonal phase at room temperature [30, 31]. Monoclinic zirconia exhibits lower compressive stresses, typically between −50 and −150 MPa. The transformation from t ZrO_2 to m ZrO_2 partially relaxes internal stresses through volume expansion, thereby reducing the overall residual stress level in the coating [32]. Furthermore, the $\sigma_{m\text{-}ZrO2}\approx 70$ MPa is lower than the residual stress obtained for the tetragonal ZrO_2 phase (~86 MPa), indicating effective stress relaxation associated with the tetragonal-to-monoclinic (t→m transformation, as reported in related coating systems [18, 33]. This noticeable reduction in residual stress, primarily attributed to its lower Young's modulus and plays a critical role in mitigating coating cracking and delamination. In the context of accident tolerant fuel cladding, the presence of monoclinic ZrO_2 contributes to enhanced mechanical stability under thermal and irradiation-induced stresses. In the other words, the residual stress–hardness relationship in the Cr–Zr coating can be understood through the combined effects of Taylor elastic stress, Hall–Petch strengthening, and Williamson–Hall microstrain. High dislocation density in the nanocrystalline coating generates large elastic interaction fields, producing significant Taylor stress that contributes directly to compressive residual stress measured by XRD. Simultaneously, nanoscale grain size enhances Hall–Petch strengthening, further increasing resistance to deformation. In contrast, the Zr substrate exhibits lower

dislocation density and larger grains, allowing stress relaxation via dislocation motion rather than elastic storage.

This distinction explains the high hardness and compressive stress state of the coating relative to the substrate.

Finally, in terms of stress magnitude, the residual stresses follow the approximate order:

$$\text{Zr (metallic)} < \text{m-}ZrO_2 \approx$$

$$Cr_2O_3 < \text{Cr (metallic)} < \text{t-}ZrO_2$$

In fact, Taylor elastic stress, originating from dislocation–dislocation interactions, constitutes the primary contributor to the measured compressive residual stress, as it directly stores elastic strain energy within the lattice. Phase transformation and thermal mismatch stresses also contribute through lattice parameter misfit across phase boundaries and interfaces. In contrast, Hall–Petch strengthening does not directly generate measurable residual elastic strain but instead governs resistance to plastic deformation by grain boundary strengthening.

Table 1. Residual stress of different phases calculated based on the estimated lattice strain from XRD

Phase	Crystal Structure	Main XRD Peak (hkl)	2θ (deg)	FWHM (deg)	Crystallite Size (nm)	Microstrain ε ($\times10^{-3}$)
Cr	BCC	(110)	~44.4	0.42	38	0.62
Cr_2O_3	Rhombohedral	(104)	~33.6	0.55	24	0.88
Zr	HCP	$(10\bar{1}0)$	~35.2	0.31	75	0.28
t-ZrO_2	Tetragonal	(101)	~30.2	0.68	15	1.10
m-ZrO_2	Monoclinic	$(11\bar{1})$	~28.1	0.47	32	0.52

Continuation of Table 1:

E (GPa)	ν	Taylor Stress (MPa)	Hall–Petch Stress (MPa)	Phase / Thermal Stress (MPa)	Residual Stress (XRD) (MPa)	Stress Nature	Role in ATF
279	0.21	-120 to -200	-50 to -100	-30 to -60	-150 to -250	Compressive	Loadbearing, wear resistance
280	0.23	-40 to -80	-30 to -60	-20 to -40	≈ -100	High compressive	Oxidation barrier
99	0.34	-20 to -50	Negligible	-50 to -100	-50 to -120	Mild compressive	Stress accommodation
210	0.30	-100 to -200	-80 to -120	-50 to -150	-200 to -400	Strong compressive	Hardness, crack suppression
170	0.25	-20 to -50	-20 to -40	Stress relaxation	-50 to -150	Tensile	Stress relaxation zone

Its role is therefore indirect, acting to stabilize the stress state by suppressing dislocation motion and delaying stress relaxation. This comparison highlights that oxide phases, particularly tetragonal ZrO_2, play a dominant role in governing the compressive stress state of the coating system. A stress-balanced coating architecture delays crack initiation under LOCA and ramped temperature conditions. These results support the suitability of Cr–Zr–based coatings as protective layers for accident tolerant fuel cladding systems.

3.4. Stress–strain modeling

Based on the XRD-derived residual stresses, simplified stress–strain behavior was modeled for individual oxide phases. Residual stresses in individual oxide phases were evaluated using

XRD lattice strain analysis. Phase-specific elastic moduli reported in the literature were used to convert lattice strain into residual stress using Hooke's law:

$$\sigma = E\varepsilon$$

where E is the elastic modulus of the corresponding phase. This approach enabled direct comparison of residual stress levels among Cr_2O_3, t-ZrO_2, and m-ZrO_2 phases in the multilayer oxide system. Elastic modulus values adopted from the literature were 280 GPa for Cr_2O_3, 210 GPa for tetragonal ZrO_2, and 170 GPa for monoclinic ZrO_2 (Hutchings et al., 2005; Cao & Ouyang, 2017). From Ludwik–Hollomon the stress-strain relationship is obtained:

$$\sigma = \sigma y + K\varepsilon_p^n$$

where: K is hardening factor, n :is hardening exponential which is (0.25-0.15) for Cr, ε_p is plastic strain. For elastic areas:

$$\sigma = E\varepsilon \leq \varepsilon_y$$

It is necessary to note that these are lattice elastic strains, not macroscopic plastic strains. Therefore, the residual elastic stress can be calculated from XRD and cannot be derived directly true elongation curve (UTS). The poison ratios are listed in Table 1. Correct averaging of the residual stress of each phase:

$$\bar{\varepsilon} = \frac{1}{N}\sum_{i=1}^{N} \varepsilon i$$

$$\bar{\sigma} = \frac{E}{1+\nu}$$

Figure 4 shows residual stress values directly obtained from XRD analysis for individual phases in the Cr–Zr ATF coating. The calculated curves represent elastic and modelled responses rather than direct mechanical testing results. The oxide phases (Cr_2O_3, t-ZrO_2, and m-ZrO_2) show significantly steeper elastic slopes, indicating higher effective elastic moduli and greater intrinsic stiffness. Metallic Cr exhibits the lowest elastic slope, consistent with its FCC crystal structure, higher dislocation mobility, and enhanced elastic–plastic compliance. The Zr substrate displays intermediate stiffness, reflecting its HCP structure and lower bonding directionality compared to ceramic phases. Metallic phases (Cr and Zr) display higher strain accommodation with gradual stress increase, indicative of dislocation-mediated strain hardening (Taylor hardening). Oxide phases exhibit limited but stable strain tolerance, particularly m-ZrO_2, which acts as a mechanically stiff phase capable of sustaining compressive load without significant plastic deformation. The coexistence of t-ZrO_2 and m-ZrO_2, with differing strain response, promotes internal stress redistribution at phase boundaries, contributing to improved mechanical stability of the multiphase coating. Deviation from linear elasticity occurs at phase-specific stress levels: Cr enters the nonlinear regime at relatively low stress due to the early activation of dislocation glide. In contrast, Cr_2O_3 and t-ZrO_2 sustain higher stresses prior to yielding, reflecting restricted dislocation activity and stronger ionic–covalent bonding. The observed shift of the effective yield point toward higher stress levels is strongly influenced by compressive residual stresses measured by XRD, which delay tensile strain localization and enhance apparent yield resistance. Similar XRD-assisted approaches have been successfully applied in the mechanical assessment of ceramic and oxide coatings for nuclear applications [15, 34].

According to Figure 5, for m-ZrO_2, a pseudo-elastic–plastic response was modeled to account for stress relaxation associated with the tetragonal-to-monoclinic phase transformation. Due to the lower elastic modulus of monoclinic ZrO_2 compared to the tetragonal phase, the calculated residual stress was significantly reduced, indicating a stress relaxation effect associated with the t→m phase transformation.

The average strain obtained from different (hkl) peaks of XRD equals to:

$\bar{\varepsilon}_{t\text{-}ZrO2}=$

$0.58+0.46+0.48+0.31+0.235=0.412\times10^{-3}$

In ZrO_2 coatings $\bar{\varepsilon}_{m\text{-}ZrO_2} \approx \bar{\varepsilon}_{t\text{-}ZrO_2}$.Therefore, $\bar{\varepsilon}_{m\text{-}ZrO2}=0.41\times10^{-3}$ and the residual stress is $\sigma_{m\text{-}ZrO2}$=70 MPa, indicating significant stress relaxation associated with the t→m phase transformation.

These results indicate that the oxide layers contribute primarily to load bearing during the early stages of deformation, whereas metallic phases provide mechanical compliance.

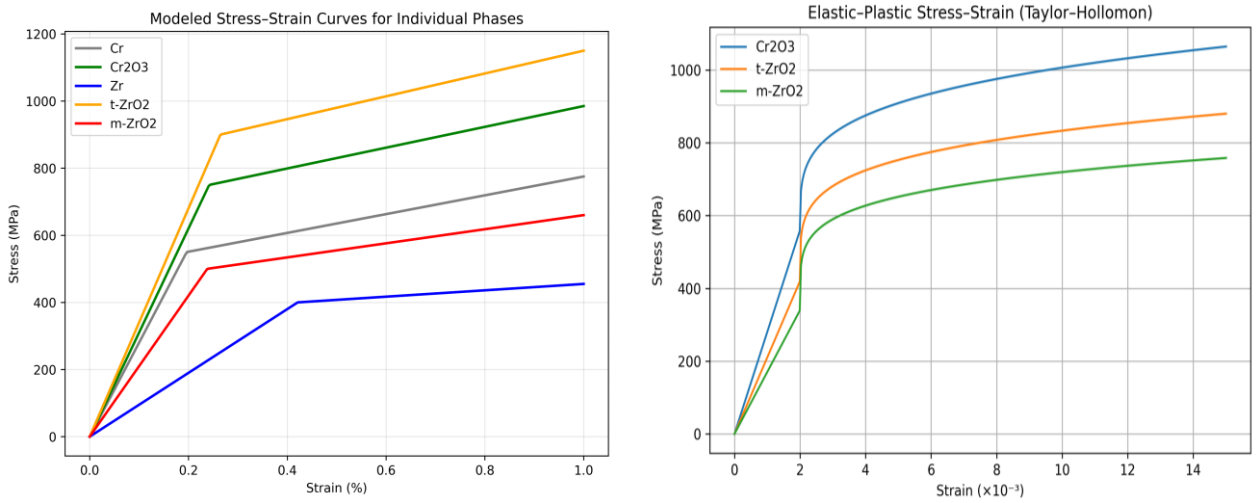

Figure 4. Modeled stress–strain responses of individual phases (Cr, Cr_2O_3, Zr, t-ZrO_2, and m-ZrO_2) in the Cr–Zr ATF coating

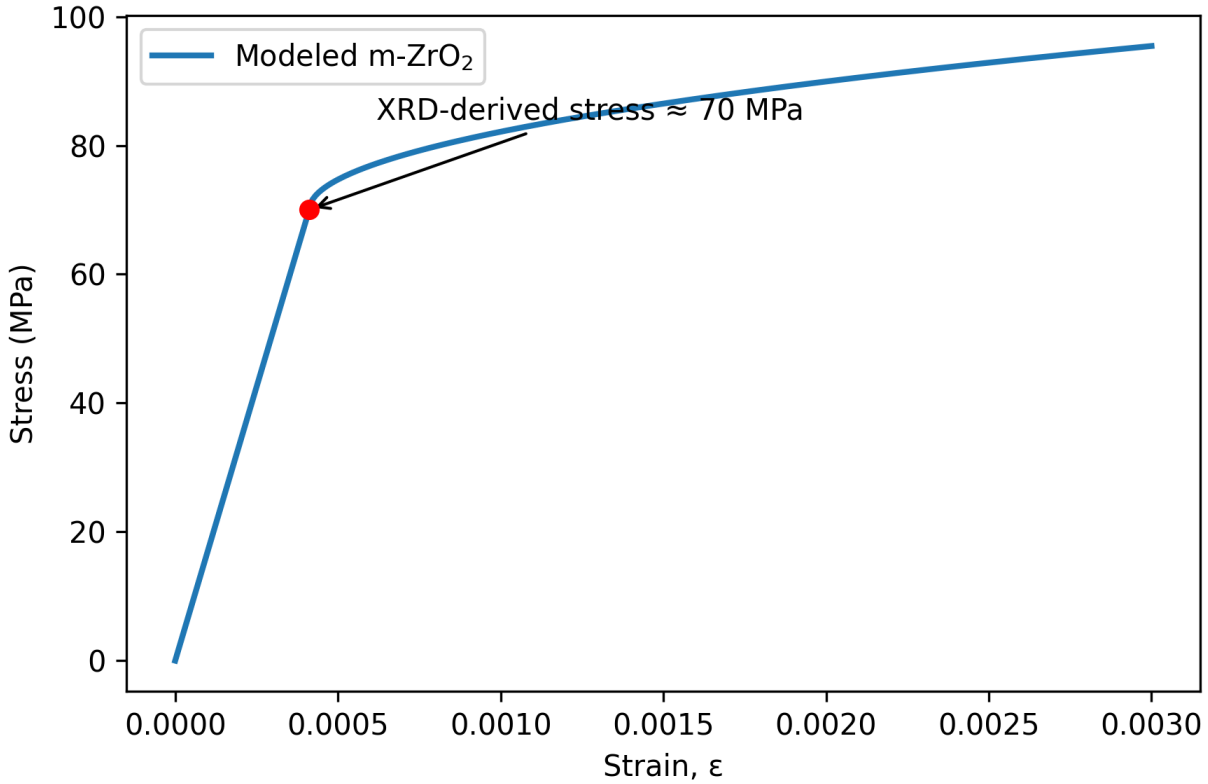

Figure 5. Modeled stress–strain curve of the monoclinic ZrO_2 (m-ZrO_2) phase in the Cr–Zr-based coating

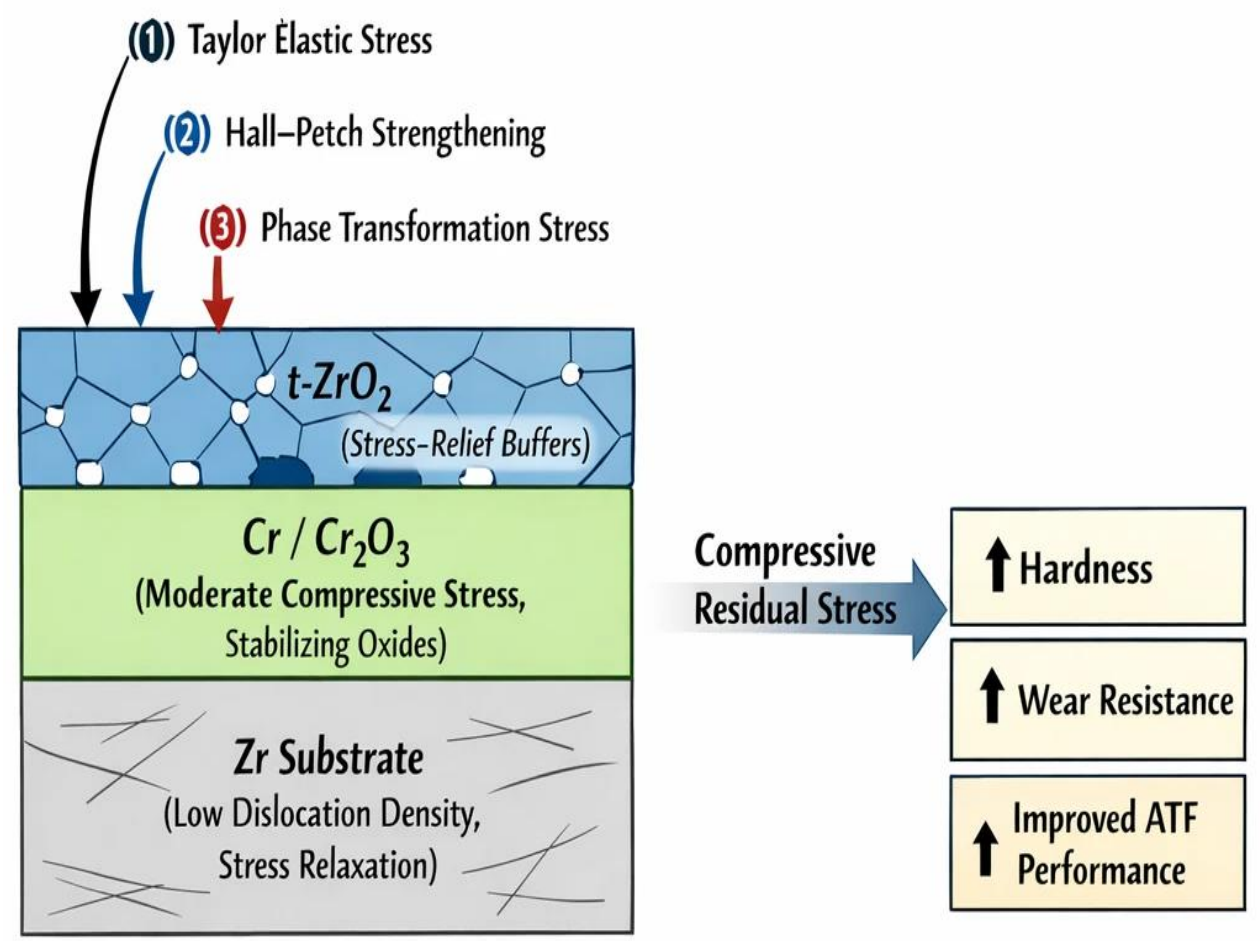

Figure 6. Scientific schematic diagram illustrating residual stress mechanisms in a Cr–Zr oxide coating on Zr substrate for ATF cladding

Figure 6 shows schematic illustration of stress generation and stabilization mechanisms in the Cr–Zr coating system for ATF cladding. The compressive residual stress arises primarily from (1) Taylor elastic stress associated with high dislocation density, (2) Hall–Petch strengthening due to grain refinement, and (3) phase transformation stress related to stress-assisted tetragonal-to-monoclinic ZrO_2 transformation. The t-ZrO_2 top layer contributes to high hardness, while the Cr/Cr_2O_3 interlayer stabilizes compressive stress and mitigates crack propagation. The Zr substrate acts as a stress-relaxation region, collectively enhancing wear resistance and ATF performance.

Although tetragonal ZrO_2 is thermodynamically stable only at elevated temperatures, its presence at room temperature in the Cr–Zr coating system is maintained through a combination of grain-size refinement, compressive stress, and interfacial constraint. Importantly, stress relaxation in t-ZrO_2-containing layers does not require complete transformation to the monoclinic phase. Localized stress-assisted tetragonal-to-monoclinic transformation can occur at grain boundaries and defect-rich regions, producing volumetric expansion that acts as an effective stress-relief buffer. In addition, the high dislocation density associated with the t-ZrO_2 layer enables partial relaxation of Taylor elastic stress through dislocation rearrangement at service temperatures. Consequently, the coating achieves a mechanically stable configuration in which high hardness is retained while catastrophic stress

accumulation is avoided. Accordingly, the high compressive residual stress observed in the Cr–Zr coating system arises predominantly from elastic strain associated with dislocation density and phase mismatch, while grain refinement serves to preserve this stress state during thermal and mechanical loading. The synergistic interaction between high compressive residual stress in the t-ZrO_2 layer, stress-stabilizing Cr/Cr_2O_3 interlayers, and the stress-relaxing Zr substrate results in a mechanically robust coating architecture. This stress balance enhances hardness and wear resistance while mitigating crack initiation and propagation under thermal cycling conditions relevant to accident tolerant fuel cladding applications. Overall, the XRD-measured residual stress state provides a direct explanation for the enhanced wear resistance of the Cr–Zr ATF coating (shown in Figure 6). The dominance of compressive residual stress in the load-bearing phases improves structural integrity, stabilizes the tribological oxide layers, and significantly extends coating durability under sliding and fretting conditions relevant to ATF cladding applications.

4. Hardness Estimation and Valid methods for estimating hardness

Residual stress plays a critical role in determining the mechanical performance of hard coatings. In Cr–Zr–based coating systems, the measured compressive residual stresses obtained from XRD analysis exhibit a strong correlation with hardness enhancement. Compressive residual stresses contribute to an apparent increase in hardness by opposing the initiation and propagation of plastic deformation. According to the modified Taylor relationship, the measured hardness H can be expressed as:

$$H = H_0 + k\,\sigma_r$$

where H_0 is the intrinsic hardness of the material, σ_r is the compressive residual stress, and k is a proportionality constant typically ranging from 0.1 to 0.3 for ceramic and ceramic–metal composite coatings [35, 36].

Role of individual phases are described below. The relatively high compressive residual stress in metallic Cr (−150 to −250 MPa) significantly contributes to increased hardness by suppressing dislocation motion during plastic deformation. This stress-induced strengthening is commonly observed in PVD Cr coatings and is associated with atomic peening and dense columnar microstructures (Huang et al., 2016). Despite exhibiting a lower compressive stress (~ −98 MPa), Cr_2O_3 enhances hardness through its intrinsically high elastic modulus and strong ionic–covalent bonding. Moreover, Cr_2O_3 acts as a stress-stabilizing phase, reducing localized stress concentration and improving load-bearing capacity during indentation [28]. Tetragonal ZrO_2 exhibits the highest compressive residual stress (−200 to −400 MPa), which plays a dominant role in hardness enhancement.

The stress-stabilized tetragonal phase restricts shear deformation and contributes to higher measured hardness values. In addition, stress-assisted phase stability delays the tetragonal-to-monoclinic transformation under mechanical loading [30].

The presence of monoclinic ZrO_2, which exhibits lower compressive stress (−50 to −150 MPa), partially relaxes internal stresses. Although this phase slightly reduces hardness, it significantly improves coating durability by preventing excessive stress accumulation and brittle cracking [31].

The coexistence of high-stress phases (Cr and t-ZrO_2) and stress-relaxing phases (Cr_2O_3 and m-ZrO_2) produces a mechanically optimized coating system.

High compressive residual stress enhances hardness and resistance to plastic deformation, while stress-moderating phases prevent premature failure due to cracking or delamination.

Consequently, the observed high hardness in Cr–Zr coatings is not solely governed by phase composition but also strongly influenced by the magnitude and distribution of compressive residual stresses within the coating architecture.

Hardness values of the oxide phases and zirconium substrate were also estimated using the empirical relationship between hardness (H) and yield stress (σ_y):

$$H \approx 3\sigma y$$

This approach allowed assessment of the relative mechanical hierarchy across the coating–oxide–substrate system. σy≈70 Mpa (from XRD results) then $H_{m\text{-}ZrO2} \approx 3 \times 70 = 210$ MPa≈0.21 Gpa. From the equation of $\sigma = \alpha \rho G b$ the hardness is equal to $H \approx 3\alpha G b \rho$, for ZrO_2: α≈0.3, b≈0.32 nm, G≈70 GPa this method directly connects the hardness to XRD microstructure.

As shown in Table 2, the effective hardness values reveal a systematic decrease from Cr_2O_3 to t-ZrO_2 and finally to m-ZrO_2. This trend reflects the intrinsic stability and mechanical role of each oxide phase formed on the Cr–Zr coated zirconium substrate.

Among the oxides, Cr_2O_3 exhibits the highest effective hardness, corresponding to its greater residual compressive stress, dense microstructure, and strong ionic–covalent bonding, which collectively enhance its resistance to deformation and oxygen diffusion [37, 38].

The tetragonal ZrO_2 (t-ZrO_2) phase, which forms at elevated temperatures, shows a lower effective hardness than Cr_2O_3.

This behavior is associated with its metastable nature and its tendency to undergo stress relaxation during cooling. As oxidation progresses, the tetragonal-to-monoclinic phase transformation results in the formation of m-ZrO_2, which exhibits the lowest residual stress and effective hardness among the oxide phases.

The volume expansion accompanying this transformation promotes local microcracking and strain accommodation, leading to significant stress relief within the oxide scale [3, 39, 40].

From a coating-scale perspective, the coexistence of Cr_2O_3 and ZrO_2 phases leads to a mechanically graded oxide structure rather than a uniformly brittle layer.

The outer Cr_2O_3-rich region acts as a hard and chemically stable protective barrier, providing effective resistance against high-temperature oxidation. In contrast, the underlying ZrO_2-rich layers, particularly those containing m-ZrO_2, exhibit reduced effective hardness and residual stress, enabling them to absorb and redistribute thermally induced stresses.

This hardness and stress gradient across the oxide scale is beneficial for mitigating interfacial stress concentrations and reducing the risk of oxide spallation during thermal transients. Such a stress-tolerant oxide architecture enhances the mechanical integrity and long-term oxidation resistance of Cr-coated zirconium claddings, which is a critical requirement for accident tolerant fuel (ATF) applications [41, 42]. The coexistence of Cr_2O_3 and ZrO_2 phases in the Cr–Zr coating results in a graded oxide system, where the hard and stable Cr_2O_3 layer provides oxidation resistance, while the stress-relieved ZrO_2 phases contribute to enhanced mechanical tolerance and spallation resistance.

Table 2. XRD-derived Effective Hardness of Oxide Phases and Substrate

Phase	σ (MPa)	H ≈ 3σ (GPa)	Discerption
Cr_2O_3	~118	~0.35	Harder oxide, higher stress
t-ZrO_2	~86	~0.26	Metastable phase
m-ZrO_2	~70	~0.21	Stress Released t→m(
Zr (substrate)	~150	~0.45	Substrate

5. Conclusion

Chromium–zirconium-based coatings were deposited on zirconium substrates using a pulsed plasma deposition system. All experiments were conducted under identical conditions, and XRD measurements were repeated to ensure consistency. Data analysis and curve fitting were performed using standard scientific software packages. The combined use of phase-resolved XRD analysis and mechanical modeling provided a comprehensive understanding of the structure–property relationships in Cr–Zr based ATF coatings. The elastic Taylor stress, Hall–Petch strengthening, and Williamson–Hall microstrain are intrinsically interconnected in the Cr–Zr coating system. In the coating, high dislocation density and nanoscale grain size result in elevated Taylor and Hall–Petch stresses, which are manifested as large compressive residual stresses measured by XRD. In contrast, the Zr substrate exhibits significantly lower dislocation density and microstrain, acting primarily as a stress-accommodating medium rather than a strengthening contributor. Overall, the stress–strain behavior confirms that the Cr–Zr ATF coating does not behave as a single homogeneous material but as a synergistic multiphase system, where:

- ductile metallic phases (Cr, Zr) provide deformation tolerance,
- stiff oxide phases supply load bearing capacity and crack resistance,
- and compressive residual stress enhances resistance to yielding and mechanical failure.

This combination is particularly beneficial under ATF operating conditions, where high stress, elevated temperature, and oxidation resistance are simultaneously required.

References

[1] Brachet J, L.S.M., Bischoff J, Palancher H, Chosson R, Pouillier E, Guilbert T,Urvoy S, Nony G, Vandenberghe T., Evaluation of Equivalent Cladding Reacted parameters of Cr-coated claddings oxidized in steam at 1200 ◦C in relation with oxygen diffusion/partitioning and post-quench ductility. Nucl Mater, 2020. 533.

[2] Kim, H.-G., et al., Adhesion property and high-temperature oxidation behavior of Cr-coated Zircaloy-4 cladding tube prepared by 3D laser coating. J. Nucl. Mater., 2015. 465: p. 531–539.

[3] Garvie, R.C., Hannink R.H. and Pascoe, R.T. , Ceramic steel. Nature, 1975. 258(5537): p. 703-704.

[4] Jérôme Chevalier, L.G., Anil V. Virkar, David R. Clarke, The Tetragonal-Monoclinic Transformation in Zirconia: Lessons Learned and Future Trends. ournal of the American Ceramic Society, 2009. 92.

[5] Bouvier, P., Tadjer, A., Monchoux, J.-P., & Chevalier, J. , Residual stresses and crack shielding in zirconia ceramics. Journal of the European Ceramic Society, 2013. 33(14): p. 2879–2887.

[6] Evans, A.G., & Hutchinson, J. W., On the mechanics of delamination and spalling in compressed films. International Journal of Solids and Structure, 1984. 20(5): p. 455–466.

[7] Sauder, C., Brusson, A., Young, J., & Lamon, J. (). Residual stresses in oxide ceramic matrix composites measured by X-ray diffraction. Journal of the European Ceramic Society, 2017. 37(8): p. 2897–2906.

[8] Munro, R.G., Elastic moduli data for polycrystalline ceramics. Journal of the American Ceramic Society. 80(8): p. 1919–1928.

[9] Anselmi-Tamburini, U., Garay, J. E., & Munir, Z. A., Fast low-temperature consolidation of bulk nanometric ceramic materials. Scripta Materialia, 2006. 54(5): p. 823–828.

[10] Beake, B.D., & Leggett, G. J. Izumi, M. Parans Paranthaman and Teruo, nfluence of residual stress on fracture and deformation during

nanoindentation of thin hard coatings. Journal of Materials Research, 2013. 28(10): p. 1349–1359.

[11] Kim, J.Y., Kang, K., Lee, Y. H., & Jang, J. , Effect of residual stress on indentation-induced cracking behavior of oxide thin films. Journal of the European Ceramic Society, 2021. 41(5): p. 2762–2770.

[12] Yilmazbayhan, A., Buscail, H., Chatzipanagiotou, H., Sauder, C., & Paillard, P., Residual stresses in thermally grown oxide scales on zirconium alloys. Acta Materialia, Inc., 2015. 86: p. 78–86.

[13] Kim, H. and J. Lee, Chromium-based coatings for accident tolerant fuel cladding: Oxidation and mechanical behavior. Journal of Nuclear Materials, 2021. 543: p. 152600.

[14] Terrani, K.A., Accident tolerant fuel cladding development: Promise, status, and challenges. Journal of Nuclear Materials 2018. 501: p. 13–30.

[15] Hutchings, I.M., Nanoindentation studies of coated systems. Surface and Coatings Technology, 2005. 200: p. 84–94.

[16] Carlotto, B., Monceau, D., Sauder, C., & Poquillon, D. , Residual stress development in oxide scales grown on zirconium alloys at high temperature. Corrosion Science, 2020. 169: p. 108598.

[17] Cao, Y., & Ouyang, J. , Role of residual stress in indentation cracking of brittle materials. Acta Materialia, 2017. 127: p. 74–85.

[18] Zhao, L., Wang, Y., Liu, X., & Zhang, T., Determination of residual stresses in oxide scales by X-ray diffraction $\sin^2\psi$ method. Corrosion Science, 2021. 187: p. 109506.

[19] Hall, E.O., The deformation and age hardening of metals. Proceedings of the Physical Society. Section B, 1951. 64(9): p. 747.

[20] Taylor, G.I., The mechanism of plastic deformation of crystals. Part I. Theoretical. Vol. Series A, 145. 1934, Proceedings of the Royal Society of London.

[21] Pantleon, W., On the evaluation of lattice strains and stresses by diffraction methods. Journal of Applied Crystallography, 2019. 52: p. 109–120.

[22] Hall, E.O., The deformation and ageing of mild steel: III – Discussion of results. Proceedings of the Physical Society. Section B, 1951. 64: p. 747–753.

[23] Petch, N.J. and . The cleavage strength of polycrystals. Journal of the Iron and Steel Institute, , 1953. 174: p. 25–28.

[24] Kim, J.H.L., B. R.; Jung, Y. G., Residual stress influence on indentation cracking and strength degradation in brittle ceramics. Journal of the American Ceramic Society, 2019. 102(6): p. 3311–3323.

[25] Williamson, G.K., & Hall, W. H. , X-ray line broadening from filed aluminium and wolfram. Acta Metallurgica, , 1953. 1: p. 22–31.

[26] Ungár, T., Dislocation density, arrangement and character from X-ray diffraction experiments. Materials Science and Engineering A, 2001. 309–310: p. 14–22.

[27] Huang, X., Yan, W., Shan, Y., Yang, K. , Residual stress evolution in oxide scales studied by X-ray diffraction. Surface and Coatings Technology, 2016. 286: p. 362–369.

[28] Gao, Y., Wang, Z., Zhang, H., Liu, Y., Residual stress evolution in oxide scales measured by X-ray diffraction. Corrosion Science, , 2018. 132: p. 213–221.

[29] Zhang, Y., Li, X., Wang, Z., Gao, Y.. Residual stress evolution in oxide scales during high-temperature oxidation studied by X-ray diffraction. Corrosion Science, 2019. 149: p. 103–111.

[30] Chevalier, J., What future for zirconia as a biomaterial? Biomaterials, 2006. 27: p. 535–543.

[31] Hannink, R.H.J., Kelly, P. M., Muddle, B. C. , Transformation toughening in zirconia-containing ceramics. Journal of the American Ceramic Society, 2000. 83(3): p. 461–487.

[32] Panicucci, L., Bertaina, S., Chevalier, J., Sauder, C. , Residual stresses and phase transformation in zirconia-based oxide scales investigated by X-ray diffraction. Journal of the European Ceramic Society, 2017. 37: p. 3027–3036.

[33] Zhang, Y., Gao, Y., Li, X., Wang, Z. , Phase-resolved residual stresses in oxide scales studied by high-temperature X-ray diffraction. Materials Characterization, 2020. 162: p. 110197.

[34] Allen, A.J., Ilavsky, J., Long, G. G., Noyan, I. C., Zhang, J., Levine, L. E., In situ studies of internal strains and stresses during deformation by X-ray and neutron scattering. Metallurgical and Materials Transactions A, 2016. 47: p. 319–341.

[35] Tsui, T.Y., Pharr, G. M., Oliver, W. C., Bhatia, C. S., Nanoindentation and nanoscratch of hard carbon coatings. Journal of Materials Research, 1999. 14(7): p. 2929–2937.

[36] Suresh, S., Giannakopoulos, A. E. , A new method for estimating residual stresses by instrumented sharp indentation. Acta Materialia, 1998. 46(16): p. 5755–5767.

[37] Pint, B.A., Dryepondt, S. N., Unocic, K. A., Lance, M. J. , The effect of substrate composition on the performance of alumina- and chromia-forming alloys. Materials at High Temperatures, 2015. 32(1–2): p. 28–39.

[38] Brachet, J.C. and C. Cabet, Behavior of chromium coatings on zirconium alloys under LOCA conditions. Journal of Nuclear Materials, 2019. 517: p. 268-285.

[39] Chevalier, J., Gremillard, L., Virkar, A. V., Clarke, D. R. , The tetragonal–monoclinic transformation in zirconia: Lessons learned and future trends. Journal of the American Ceramic Society, , 2009. 92(9): p. 1901–1920.

[40] Kim, J.H., Jang, J.-I., Pharr, G. M. (). Influence of residual stress on the mechanical response measured by nanoindentation. Journal of Materials Research,, 2018. 33(3): p. 295–305.

[41] Terrani, K.A., Pint, B. A., Parish, C. M., Silva, C. M., Snead, L. L., Katoh, Y. (). Silicon carbide oxidation in high-temperature steam environment. Journal of Nuclear Materials, 2014. 448: p. 420–435.

[42] Pint, B.A., Yeom, H., Terrani, K. A. (). High temperature oxidation of fuel cladding candidate materials in steam–hydrogen environments. Journal of Nuclear Materials, , 2018. 511: p. 99–112.